Article Identifier
DOI: 10.22032/dbt.58843
URN: urn:nbn:de:gbv:ilm1-2023isc-094:0

60th ILMENAU SCIENTIFIC COLLOQUIUM
Technische Universität Ilmenau, 4 – 8 September 2023
URN: urn:nbn:de:gbv:ilm1-2023isc:1

Fabrication of asymmetric multimode splitters in glass by planar ion exchange and laser ablation

D. Schaeffer, D. Klenkert, J. Stauch, M. Kufner, R. Foerg and J. Ebbecke

Technology Campus Teisnach Sensor Technology, Deggendorf Institute of Technology, Teisnach, 94244 Germany

ABSTRACT

The fabrication of planar lightwave circuits (PLC) using the laser-ablated ridge waveguide technique is explored. In particular, asymmetric multimode splitter structures are designed and fabricated. The experimental work is accompanied by modeling the relevant parameters. An ion exchange model determines a suitable set of ion exchange duration, temperature, electric field, and ridge geometry. In the simulation, special attention is paid to a good match of the waveguide shape between the PLC components and commercially available GRIN fibers.
Wave-optical simulations of the light propagation in the PLC devices are performed using a scalar beam propagation method. Based on the simulation, asymmetric splitter devices are designed for a variety of splitting ratios. A 70:30 splitter is fabricated and attached to optical fibers for characterization. As indicated by a low excess loss, low intrinsic waveguide losses are achieved. The experimental splitting ratio is in good agreement with the simulation.

Index Terms **–** Integrated Optics, Ion Exchange, Laser ablation, Glass waveguides

1. INTRODUCTION

Planar lightwave circuits (PLC) play a critical role in today's fiber-based data transmission networks. A well-established production method for PLC is the Na^+/Ag^+ exchange in glass [1]. It is based on the local increase of the refractive index of soda-lime glass by exchanging Na^+ from the glass with Ag^+ from an external source (e.g., $AgNO_3$ melt). This technique yields graded index waveguides that are ideally suited for the use with standard multimode GRIN fibers. However, the fabrication of certain multimode devices, such as asymmetric splitters, still poses significant challenges [2].
Usually, photolithographic masks are used to shape the paths of the optical waveguides. Additionally, an electric field is often applied to accelerate the diffusion process and to enable steeper refractive index profiles. However, this approach has significant drawbacks, as the combination of mask and electric field leads to a distortion of the diffusion pattern at the mask edges, which yields undesirable bone-shaped waveguides [3,4].
Morand et al. [5] demonstrated an alternative manufacturing method, which abandons the lithographic mask and instead relies on the physical removal of parts of the glass substrate to form waveguides. In this approach, a Na^+/K^+ ion exchange is conducted over the whole substrate surface. Afterwards, a precision saw is used to cut two parallel grooves into the glass. The ridge remaining between these grooves forms the waveguide.
In a previous work [6], we modified this approach. In the first ion exchange step, Ag^+ from an $AgNO_3$ melt is used instead of K^+ as the exchanging species since Ag^+ allows for an increase in the refractive index up to a factor of 10 larger than K^+ [7]. Additionally, an electric field is

applied across the glass substrate to accelerate the process. This results in a planar waveguide at the surface. Two parallel grooves are cut through the Ag^+ enriched layer by laser ablation, with a ridge remaining in the middle. The laser ablation process allows for greater freedom of design compared to the use of a saw. In an additional step, a second ion exchange with Na^+ is performed by putting the substrate inside a $NaNO_3$ melt. This removes Ag^+ from the surface of the ridge, thus insulating the Ag^+ enriched waveguide from surface defects, which might cause optical losses. In Figure 1, this fabrication process is shown schematically [6].

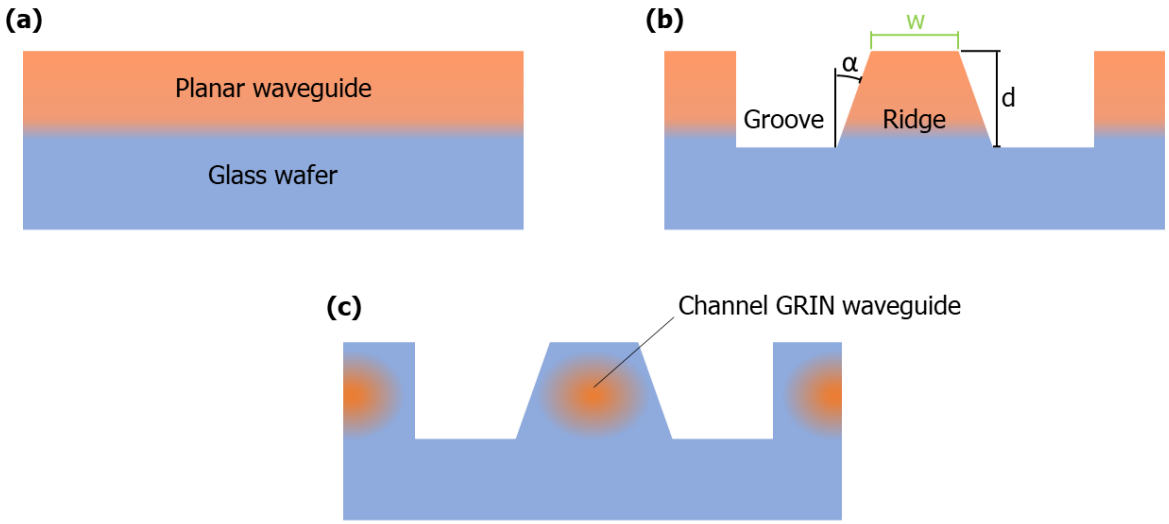

Figure 1: Schematic view of the manufacturing process. (a) Plane waveguide at the glass surface generated by Na^+/Ag^+ ion exchange. (b) Two parallel grooves ablated into the substrate via ultrashort pulse laser. A ridge remains between them. (c) Second ion exchange with Na^+ ions creates a roughly circular waveguide in the center of the ridge and shapes the refractive index profile. Based on [6].

2. METHODS

2.1 Experiments

In the present work, 6-inch glass wafers with a custom composition suitable for ion exchange (similar to BGG-31) are used as a substrate. The wafer is placed in a vertical tube furnace. To allow a field-assisted first ion exchange with $AgNO_3$, the glass's top and bottom surfaces are galvanically isolated.

The laser ablation is conducted with a GFH GmbH GL.compactII ultrashort pulse laser micromachining system. Structuring the grooves and dicing the wafer into individual chips is done in a single clamping setup. This saves processing effort and ensures minimal offset between the cut edges and the structures.

The individual chip carrying the surface waveguide is placed in a $NaNO_3$ bath for the second exchange. Subsequently, it is cleaned and bonded with a glass cover to protect the edges during the end-face preparation. After grinding and polishing, we measure a surface roughness Ra between 2 nm and 7 nm across all finished waveguide interfaces.

To image the waveguide profiles, we use a Thermo Fisher Scientific Phenom XL SEM in backscatter mode. This allows the 2D imaging of the Ag^+ concentration along the polished end faces.

Fiber ports mounted with GRIN fibers (Ø50 µm Core / Ø125 µm Cladding, OM4, 0.2 NA) are attached to the splitter utilizing a custom-made waveguide aligner. Therefore, the fiber core is illuminated, and an optimizer is used to drive the apparatus automatically to maximize the

summed output power of the splitter device. For the bonding process, we choose optical Norland 148 UV adhesive [8].
Two fiber ports are bonded together to estimate the connection losses. Measurements with an LED show that the loss for a single bonding layer is 0.2 ± 0.1 dB.

2.2 Simulation

The simulation of the ion exchange process is conducted using the model described in [4] implemented with Comsol Multiphysics. This model is used to calculate two-dimensional Ag^+ concentration maps over the cross-section of the ridge waveguides by solving the coupled diffusion equations for Ag^+ and Na^+.
For the simulation of light propagation through a PLC, Ag^+ concentration maps perpendicular to the optical axis are simulated. The Ag^+ distribution is then converted to a refractive index profile assuming a linear relationship between the two [7]. Based on the refractive index maps, the light propagation is calculated using a 3D scalar implementation of the finite-difference beam propagation method (FD-BPM) [9]. To achieve high accuracy of the FD-BPM, a step size of 200 nm is used in the direction of the optical axis and a step size of 100 nm perpendicular, while the wavelength for the simulation is 850 nm.
For realistic devices, a lot more refractive index maps are required for the BPM simulation than can be reasonably calculated using the diffusion model. Therefore, interpolation between the calculated maps has to be used. To obtain reliable results with the BPM, a suitable electric field is defined as an optical input. We calculate all guided modes of a 50 µm step-index fiber and add them up. The resulting electric field is then used as an input field to the BPM simulation of a 10 mm long segment of the 50 µm GRIN fiber, which is used in the experiments. Its output electric field is used as an input field for all BPM simulations in this work.

3. LINEAR WAVEGUIDES

Linear waveguides are simulated and fabricated to develop suitable process parameters for a good optical match to commercially available 50 µm GRIN fibers. Using the simulation, the ridge width, and depth, along with the exchange parameters for both ion exchange steps, are varied to realize a mostly circular profile of 50 µm diameter for the high-power waveguide.
For the first exchange step, a duration of 3 hours at 294°C with an electric field of 23 kV/m across the wafer is employed. This yields a homogeneously Ag^+ enriched layer of about 55 µm thickness at the substrate surface.
Based on fabrication tests, a ridge angle α of 25° was chosen to ensure the steepest possible flank, while maintaining a good surface quality. Additionally, the depth d was set to 75 µm, with two different waveguide widths being tested, 25 µm and 15 µm. For the simulation, the assumed exchange temperature is set to 297.5°C to achieve the same diffusion depth as in the experiment. This might be explained by temperature fluctuations in the repeatability of the process. Figure 2 shows a comparison of the simulated and experimentally determined Ag^+ concentration map, measured with backscatter SEM, after the laser ablation step for both ridges. The slight temperature increase of 3.5 K in the simulation reproduces the experimental depth profile of the concentration very closely.
The second ion exchange is conducted for 10 hours at 315 °C without an electric field. The resulting Ag^+ concentration distributions for the simulation, as well as the experiment, can be seen in Figure 3. It can be seen that the zone of maximal concentration is at a greater depth in the experiments than predicted by the simulation. However, the overall shape shows a good agreement with the simulation enabling the fabrication of waveguide ridges, which are expected to have low coupling losses to optical fibers.

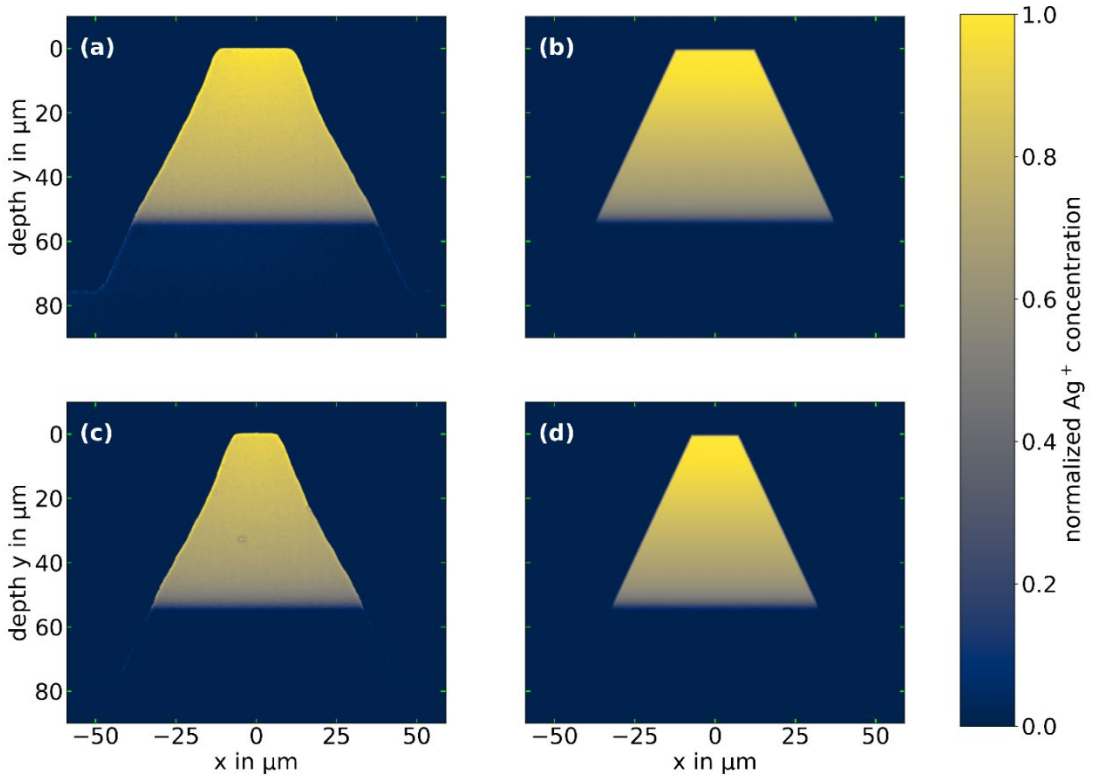

Figure 2: Comparison of the simulated and experimental Ag^+ concentration in waveguide ridges of different widths directly after laser ablation. 25 µm top width: experimental (a); simulation (b). 15 µm top width: experimental (c); simulation (d).

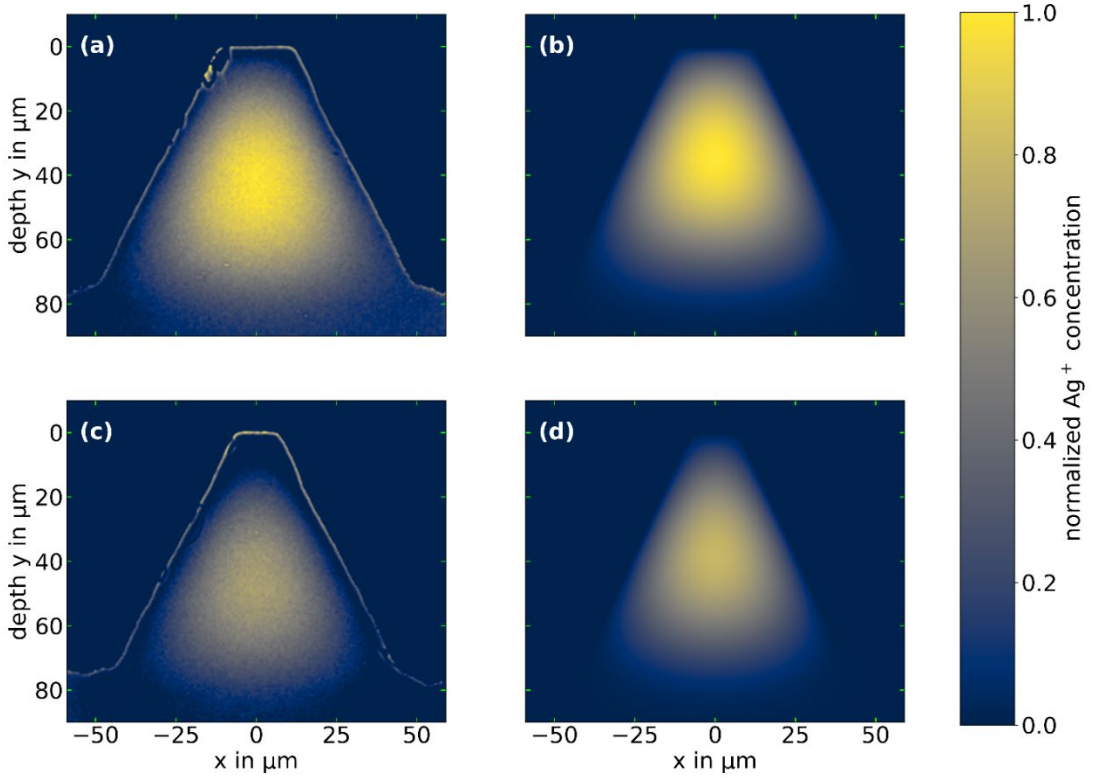

Figure 3: Comparison of the simulated and experimental Ag^+ concentration in waveguide ridges of different widths after the second ion exchange. 25 µm top width: experimental (a); simulation (b). 15 µm top width: experimental (c); simulation (d).

4. SPLITTER DESIGN

Splitter structures are designed using the previously established geometries for the waveguide ridges. These devices have one input waveguide, which branches into two waveguides that move away from one another on mirror-symmetric paths (see Figure 4). To ensure low bending losses, these paths follow a distinct function, which consists of a circular arc, followed by a polynomial. Overall, the splitter device has a length of 20 mm, and on the output side, the waveguide centers are separated by 250 µm to allow the attachment of optical fibers [8].
To achieve an asymmetrical splitting of the optical power, the two waveguide branches on the output side are structured with different diameters by changing the width of the ridges. Another requirement for the waveguide diameter is minimizing the coupling losses, which are due to a mismatch of the diameter and refractive index between waveguides and the attached optical fibers. Therefore, the ridge width of the input and the high-power output waveguide is chosen to be identical and optimized for a good optical match to the attached fibers. The low-power waveguide is then designed with a smaller diameter optimized for achieving the desired splitting ratio.

Figure 4 shows the simulated topography of such a splitter structure.

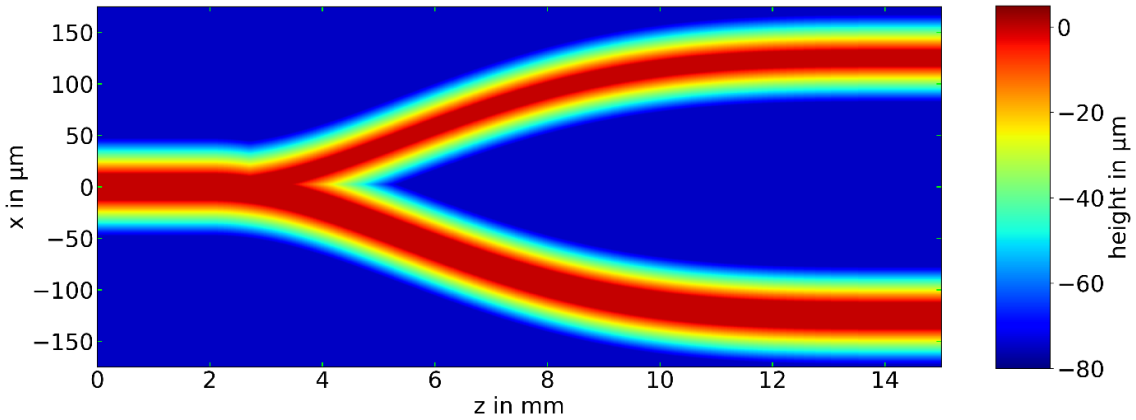

Figure 4: Intended topography of the asymmetric splitter structure.

To examine the possibility of achieving asymmetric splitting ratios, we simulate the light propagation for a series of splitters with different low-power waveguide widths w_2. In contrast, the width w_1 for the high-power waveguide ridge is set at 25 µm. For these simulations, 95 Ag^+ concentration maps are calculated for each splitter. The Ag^+ concentration is converted to refractive indices by assuming the maximum concentration after the first exchange corresponds to a refractive index increase of 0.14.
The BPM is performed based on these refractive index maps. Figure 5 (a) shows the simulation of the refractive index distribution over the splitter structure, while (b) shows the propagation of optical power. Both simulations are conducted in three dimensions and integrated over the y-direction to generate the plots.

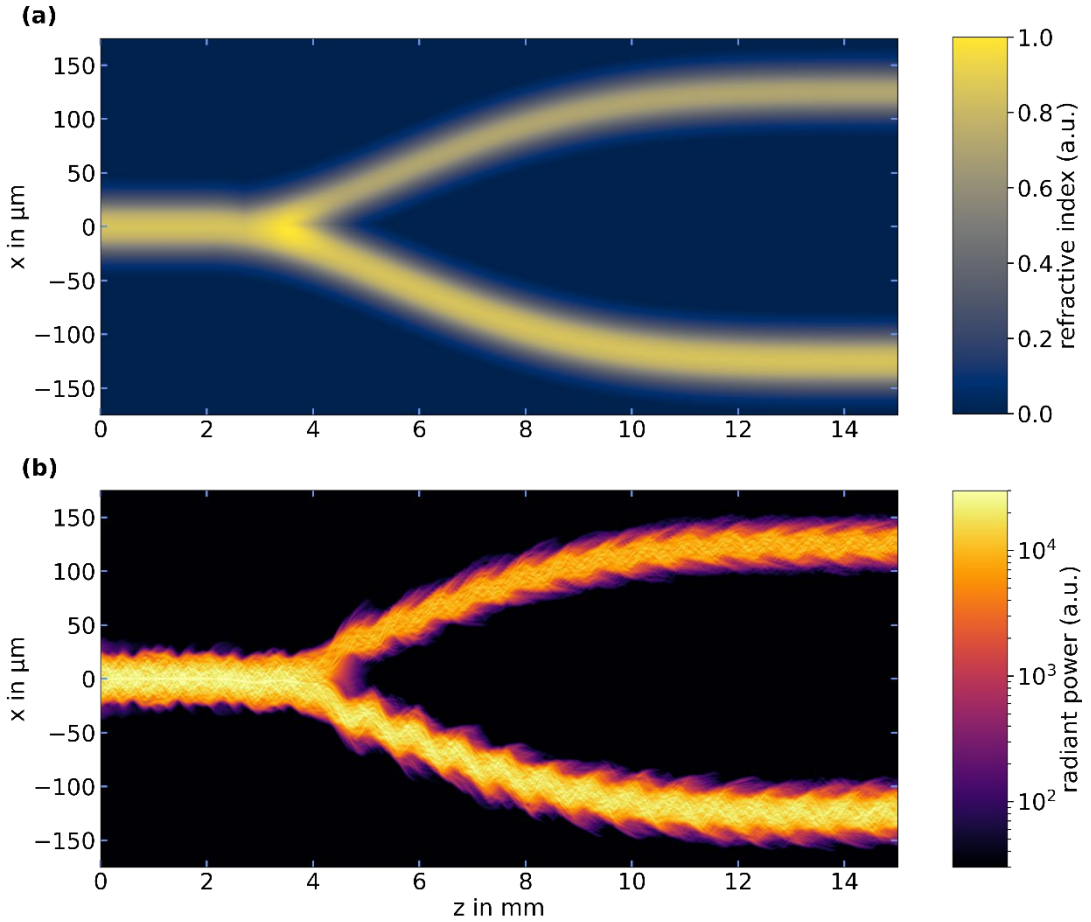

Figure 5: Simulation of an asymmetric splitting structure. (a): Simulation of the refractive index distribution. (b): Simulation of the light propagation using BPM.

A first-order approximation of the splitting ratio can be calculated based on the Ag^+ concentration distribution in the wide waveguide WG1 and the small waveguide WG2. This avoids the calculation of a full BPM simulation of the splitter structure, with only one concentration map of both waveguide ridges being required. By integrating the squared Ag^+ concentration c_{Ag} over the cross-section of each waveguide, we can calculate the approximation of the splitting ratio as follows:

$$\text{Splitting ratio} \approx \frac{\int_{WG1} c_{Ag}^2 dA}{\int_{WG1} c_{Ag}^2 dA + \int_{WG2} c_{Ag}^2 dA}$$

In Figure 6, the resulting splitting ratios from this approximation are shown alongside the ratios simulated by using BPM. Both methods yield the expected splitting ratio of 50:50 for a width of the low-power ridge of 25 µm (i.e., both ridges are equally wide). For smaller widths w_2, the approximation suggests splitting ratios, which are consistently 3-4 percentage points lower than the simulation. A splitting asymmetry of 90:10 can be achieved if the low-power ridge has a vanishing top width. Between these extremes, a nearly linear progression is observed.

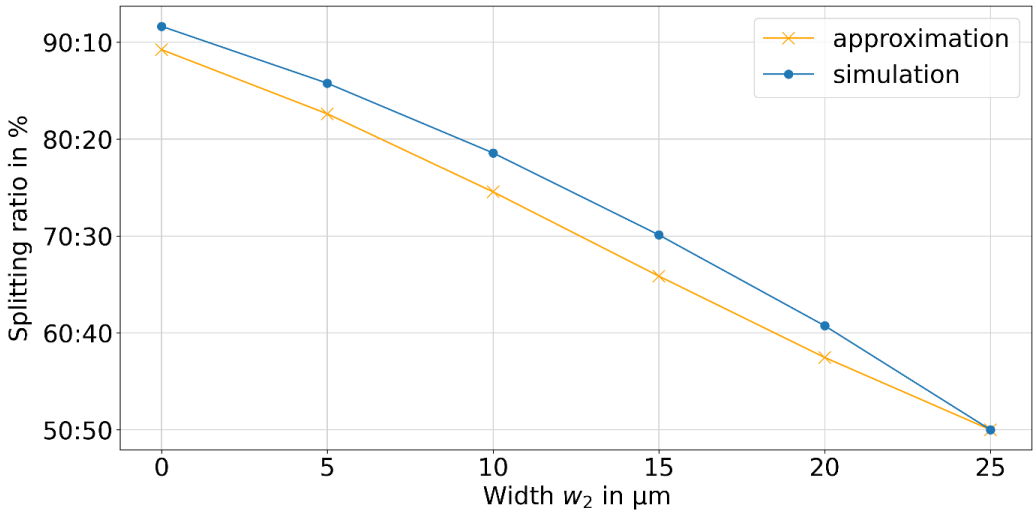

5. FABRICATION AND CHARACTERIZATION OF SPLITTERS

A splitter device with an intended splitting ratio of 70:30 is fabricated according to the previous design considerations. After the laser ablation process, a height map of a section of this structure is recorded using confocal laser scanning; the result is shown in Figure 7.

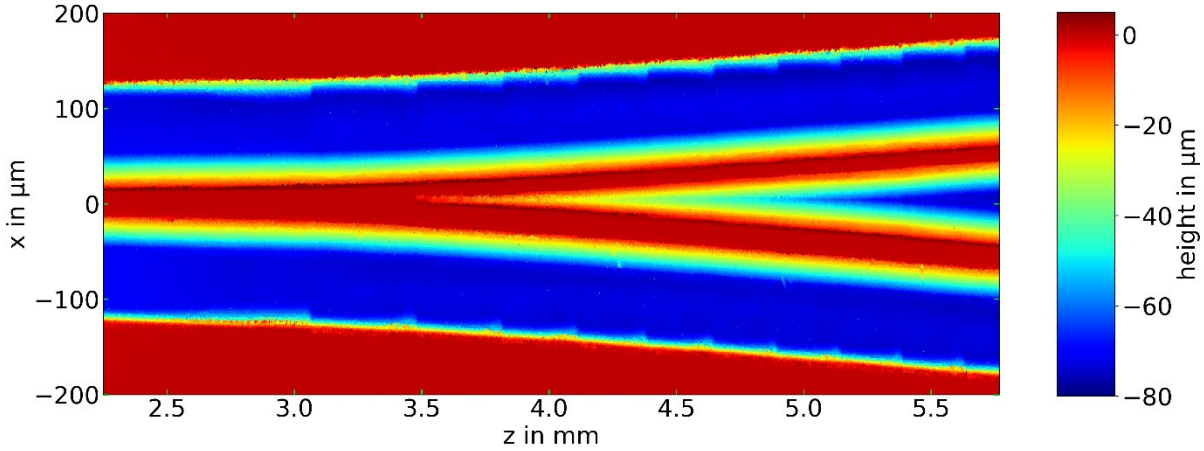

The sidewalls of the waveguide ridges are uniformly descending, and no discontinuities along the waveguides are observed. However, there are significant discontinuities on the opposite side walls of the trenches. Here, the material was coarsely removed to save process time since these faces do not directly influence the quality of the optical waveguides.
Subsequently, the second ion exchange is performed, resulting in waveguide profiles corresponding to those shown in Figure 3. The splitter chip is post-processed, and its input is coupled to a GRIN fiber. Using an 850 nm LED as the light source, the output powers are measured (see Table 1) and compared to the simulation results.

The splitting ratio is in good agreement with the intended numbers. The losses, on the other hand, are significantly higher than predicted by the simulation. This can be explained by the fact, that the only loss mechanism the simulation accounted for, was the waveguide bending and the branching. However, these losses are negligible compared to other loss mechanisms, including coupling losses between fiber and PLC (about 0.2 dB) and surface roughness of the waveguides.
To determine the splitter behavior in modern datacom networks, the two outputs were coupled to the same GRIN fiber type via fiber ports. The measurement was repeated with the LED and an 850 nm VCSEL as a light source (see Table 1, marked with *).

Table 1: Optical properties of the asymmetric splitter device. The input was coupled to a 50 µm GRIN fiber.

Optical properties	Simulation	LED	LED*	VCSEL*
Excess loss (dB)	0.0	0.7	1.4	0.8
Splitting ratio (%)	70:30	71:29	70:30	81:19

**inputs and outputs were coupled to optical 50 µm GRIN fibers.*

The VCSEL excites mainly modes of low order near the fiber core center, while the LED also excites modes of higher order, which propagate near the fiber core edge [10]. As a result, the VCSELs experience significantly lower intrinsic coupling losses between fiber and PLC and less influence from the non-smooth ridge surfaces. Moreover, the splitting ratio is more asymmetric compared to the LED due to the different modal fields. This can be explained by the more core-centered VCSEL field, which more closely follows the wider waveguide branch with its higher refractive index.

6. CONCLUSION

The laser-ablated ridge waveguide technique is further investigated to determine its suitability for the fabrication of PLC components. A simulation workflow is established to examine the optical properties of such components in silico. It consists of an ion exchange simulation based on the diffusion equation to determine 2D refractive index distributions, which are used in the second step to calculate light propagation through the components using a 3D-BPM implementation.
Based on the simulation, a suitable ridge geometry and exchange parameters are established to ensure a good optical match to commercially available 50 µm GRIN fibers. Using the BPM, the correlation of waveguide ridge widths and the splitting ratio is investigated, revealing a nearly linear dependence. Using these results, a splitter structure with an intended splitting ratio of 70:30 is chosen for fabrication.
Measurements of the Ag^+ concentration distributions inside the ridges after the laser ablation and after the final ion exchange step are conducted using backscatter SEM. They show a good agreement with the preliminary simulations. Finally, the splitter structures are connected to optical fibers on the input side to determine their properties. These measurements reveal a splitting ratio of 71:29, matching the BPM simulation, and an excess loss of 0.7 dB, which is acceptable for these types of devices.
After fiber-coupling the output side, losses of 1.4 dB and 0.8 dB were recorded, respectively, using a LED and a VCSEL as light sources. Due to the different modal fields of these two sources, varying splitting ratios are recorded with 70:30 for the LED and 81:19 for the VCSEL.

We have demonstrated the suitability of the laser-ablated ridge waveguide technique for the fabrication of low-loss asymmetric multimode splitter devices. Thus, paving the way for this fairly new approach to be used more widely as a means of manufacturing complex PLC devices.

REFERENCES

[1] Broquin, J. E., & Honkanen, S. (2021). Integrated photonics on glass: A review of the ion-exchange technology achievements. *Applied Sciences*, *11*(10), 4472.

[2] De Oliveira, A. D., Wilson, M. G. F., & Parriaux, O. (1981). Stripe waveguide Y-intersection as efficient coupler for multimode optical communication systems. *Electronics Letters*, *2*(17), 100-101.

[3] Mrozek, P. (2012). Numerical and experimental investigation on Ag+–Na+ field assisted ion-exchanged channel waveguides. *Applied Optics*, *51*(20), 4574-4581.

[4] Schaeffer, D., Klenkert, D., Stauch, J., Brand, F., Foss, W., Schwietering, J., ... & Kufner, M. (2021). Simulation of field-assisted ion exchange in glass regarding the space-charge density and pseudo-mixed-alkali effect. *Applied optics*, *60*(22), 6632-6638.

[5] Morand, A., Kaur, Y., Gri, M., Ardila, G., & Benech, P. (2019, March). Glass integrated optic waveguides combining optical grade dicing and ion-exchanged planar waveguide. In *Integrated Optics: Devices, Materials, and Technologies XXIII* (Vol. 10921, pp. 57-64). SPIE.

[6] Schäffer, D., Klenkert, D., Stauch, J., Kasberger, A., Kufner, S., Kufner, M., & Foerg, R. (2021, September). Planar ion exchange and laser ablation for prototyping of integrated optics in glass. In *Optical Design and Engineering VIII* (Vol. 11871, pp. 93-101). SPIE.

[7] Findakly, T. (1985). Glass waveguides by ion exchange: a review. *Optical engineering*, *24*(2), 244-250.

[8] Schaeffer, D., Klenkert, D., Stauch, J., Foss, W., Haaf, S., Foerg, R., & Kufner, M. (2022). Asymmetric optical multimode splitters by field-assisted ion exchange using patterned mask openings. *Optics Express*, *30*(22), 39353-39360.

[9] Pedrola, G. L. (2015). *Beam propagation method for the design of optical waveguide devices*. John Wiley & Sons.

[10] Peng, G. D. (Ed.). (2019). *Handbook of Optical Fibers* (Vol. 301). Berlin/Heidelberg, Germany: Springer.

CONTACTS

D. Schaeffer
email: daniel.schaeffer@th-deg.de
ORCID: https://orcid.org/0000-0003-2573-1128

D. Klenkert
email: daniel.klenkert@th-deg.de
ORCID: https://orcid.org/0000-0003-3528-8975